The first LWA Swarm Calibrator Survey

C. A. TAYLOR, G. B. TAYLOR, J. DOWELL, AND S. PEZZAIOLI Land Tuniversity of New Mexico

ABSTRACT

The LWA Swarm is the aperture synthesis telescope consisting of interconnected LWA Stations autonomously making joint observations (J. Dowell & G. B. Taylor 2018). In 2024, the Long Wavelength Array (LWA) collaboration completed commissioning for the LWA – North Arm, a 64-element 'swarm' station, and construction is underway to build two additional LWA swarm stations in Arizona and Texas. By early 2026, the LWA Swarm will be a six station long baseline interferometer, capable of arcsecond resolution imaging with millijansky sensitivity. Here we use the 3-element interferometer consisting of LWA1, LWA-SV, and LWA-NA to survey 30 radio sources as candidate calibrators for the LWA Swarm. Of these 30 sources observed we find 25 viable calibrators and present images of all sources at 66 MHz. Based on the properties of the observed calibrators, we conclude that many other suitable calibrators will be available to the LWA Swarm. In anticipation of the availability of this new instrument, we provide a preliminary guide to observing and calibrating LWA Swarm data.

Keywords: Calibration (2179) – Radio Sources (1358) – Very Long Baseline Interferometry (1769)

1. INTRODUCTION

Cosmic radio signals detected by terrestrial telescopes are subject to atmospheric distortions, introducing a unique and dynamic refractive index along the line of sight. For an interferometer or distributed array telescope, this can corrupt correlated visibilities by introducing time-variable terms in the delay and phase to each antenna or detector. Path length changes due to refraction are proportional to the free electron content of the ionosphere and frequency as n_e/ν^2 , making the effects especially prominent at low radio frequencies (< 100 MHz) and during daytime observing conditions when the ionosphere is ionized by solar radiation. To mitigate these effects, radio interferometers observe compact calibrator sources, such as bright radio galaxies, to solve for solutions to propagation irregularities. Thus, an interferometer must have a catalog of calibration targets to reference when undertaking science observing campaigns.

The Long Wavelength Array (LWA) is an interferometer array telescope collaboration comprised of 'stations' distributed across the Southwestern United States. These stations observe over a frequency range of 3–88 MHz and are composed of a pseudo-random distribution of dual-polarization dipole antennas spread across an ~100m aperture (G. B. Taylor et al. 2012). Each station is a digital

Email: ctaylor98@unm.edu

37

38

39

40

41

42

43

45

49

51

52

54

55

57

58

60

61

63

67

69

70

71

72

beamforming aperture array capable of targeted observing and all-sky imaging on its own, or in cooperation with other LWA stations to form an interferometer. Continued improvement in radio astronomy technology, since the construction of the first LWA station in 2012, has allowed subsequent stations to incorporate new features and improved flexibility. For this reason, all LWA stations are slightly different in their construction, but fundamentally are maintained and operated using the same libraries of software^b. LWA1, located near the Karl G. Jansky Very Large Array (VLA) control building, and LWA-SV, located at the Sevilleta National Wildlife Refuge, are both 256-element stations. OVRO-LWA, hosted at the Owens Valley Radio Observatory and operated by Caltech, is a 352-element station with a core of 243 elements and 109 elements at long baselines up to ~2.4 km for arc-minute scale imaging. The newest station commissioned is LWA-NA, a smaller 64-element 'swarm' station located near the end of the VLA North arm (C. A. Taylor et al. 2025).

The LWA Swarm is the long baseline aperture synthesis telescope, comprised of interconnected LWA stations autonomously making joint observations, based on the Swarm Telescope Concept described in J. Dowell & G. B. Taylor (2018). By the end of 2025, the LWA will have added two 64-element swarm stations, one located at Meteor Crater in Arizona (LWA-MC, operated by Arizona State University) and another at the Comanche Spring Astronomy Campus outside Crowell, Texas (LWA-CS, operated by Texas Tech University). When these stations enter service, the 6-station LWA interferometer will have baseline lengths up to approximately 1700 km (between OVRO-LWA and LWA-CS) and deliver ~1 arcsecond angular resolution or better across the LWA band. The LWA has always been an open-skies radio telescope, and the LWA Swarm will be its interferometry extension, with observing time available to the community through the annual LWA Call for Proposals^c.

Interferometry between separate LWA stations has been available for many years, but in a slightly different context, as exemplified by two projects that motivate this work. I. Davis et al. (2020) investigated several flaring UV Ceti-type variable M-dwarfs using the single baseline interferometer between LWA1 and LWA-SV. These observations identified evidence of a flare from EQ Pegasi in both Stokes I and V, but were unable to provide higher significance measurements with the LWA interferometry mode without the baselines needed to provide increased sensitivity, aid in calibration, and provide imaging capabilities. Imaging is possible when observing in the Expanded LWA (ELWA) mode – a combination of the VLA 4m-band system, LWA1, and LWA-SV – such as in D. Ruan et al. (2020), where a search for off-pulse emission from PSR B0950+08 found a pulsar wind nebula. Despite an angular resolution of 8.2 arcseconds with mJy sensitivity, the ELWA mode has seen limited efficacy due to correlating self-generated radio frequency interference (RFI) caused by the antenna control units (D. Ruan et al. 2020; L. Tremou et al. 2024). While mitigation for this RFI is scheduled to be completed before the next VLA A-configuration in February 2026, the LWA Swarm is no longer bound to this system to access high-resolution imaging with the addition of the LWA-NA station. Therefore, identifying sufficiently bright calibrator sources within the detection limits of the LWA Swarm is a high priority as the collaboration expands to include more stations and longer baselines. There are two other primary long baseline interferometers operating at MHz radio frequencies to compare to the developing LWA Swarm, the Murchison Widefield Array (MWA) and the International LOFAR Telescope (ILT). The MWA achieves 2 arcminute imaging resolution in the 120–168 MHz band, and expects to see a factor of two improvement to this measure after commissioning the in-

b https://github.com/lwa-project

c https://leo.phys.unm.edu/~lwa/proposals.html

progress Phase II/III upgrades (R. B. Wayth et al. 2018). While the ILT can push further than this using its High Band Array (HBA: 120-240 MHz), achieving sub-arcsecond imaging in the Northern sky, the corresponding Low Band Array (LBA; 10-80 MHz) is limited to imaging only the brightest radio galaxies at this resolution (O. Wucknitz 2010; L. K. Morabito et al. 2016; C. Groeneveld et al. 2022). The LWA Swarm, realized as a 6-element heterogeneous interferometer, is expected to be able to match the angular resolution and sensitivity of the ILT LBA, but with increased access to the Galactic Center at -37° Declination. This region will be accessible to the future SKA-Low telescope being built at the CSIRO Murchison Radio-astronomy Observatory, but this instrument is not scheduled to be complete until 2030.

In the following sections, we describe the first survey of long baseline calibrator sources for the LWA Swarm Interferometer. Section 2 describes the ELWA correlator development and its application to LWA-only interferometry. Next, Section 3 makes estimates of the expected sensitivity of the 3-element interferometer used in this study. Section 4 outlines the selection criteria for the LWA Swarm Calibrator Survey, the observation scheduling structure, and details the observations themselves. Section 5 outlines the overall calibration and imaging methodology. Section 6 describes the results of the survey. Section 7 discusses the implications of these results to the expansion plans of the LWA and, lastly, Section 8 details future observing plans for when the LWA Swarm is back online.

2. EXPANDED LWA CORRELATOR

The ELWA observing mode allows for coordinated observing using the Expanded VLA 4m-band system and the nearby LWA stations operating in New Mexico. In this observing mode, the VLA sends pointing triggers to available LWA stations to follow along with beamformed observations (~ 30 s delay to trigger LWA). VLA antennas record the observation in the VLBI Data Interchange Format (VDIF) with 8 MHz of bandwidth (real, upper side band), and available LWA stations observe in a special 9.8 MHz DRX tuning (4+4-bit complex). Observations of this type are scheduled through the VLA scheduler tools and must be proposed during VLA observing cycles, ideally in A-configuration. The ELWA software correlator^d was designed to accommodate merging these differing bandwidths, data formats, and feed polarization bases, then perform timing alignment, apply corrections for the LWA antenna gain pattern, and correlate this amended baseband data between the two instruments. The correlator itself is an FX-style, CPU-only implementation that manages and distributes correlation jobs across three servers on the LWA Users Computing Facility (UCF). While his mode provides sensitivity and imaging that is superior to single-station LWA observing, it also reduces each LWA station's available bandwidth by 75%. Thankfully, the ELWA software correlator was not exclusively designed for LWA+VLA interferometry observations but is flexible for processing the full bandwidth of LWA-only DRX data when observing in the LWA Swarm mode.

LWA Swarm observations are configured by observers using a session scheduler GUI^e to produce Interferometry Definition Files (IDF). An IDF encapsulates all of the station direction for an LWA Swarm run, namely the scan beam pointings and duration, spectral resolution, integration time, LWA analog filter, and digital gain settings. Once an IDF is approved for scheduling by the LWA validator tool, Session Definition Files (SDF; used for single-station LWA observations) are automatically created from the IDF and propagated to the individual stations. This creates a layer of redundancy

76

77

78

80

81

83

84

87

90

91

92

93

94

95

97

98

99

100

101

102

103

104

105

106

107

108

109

110

111

112

114

d https://github.com/lwa-project/eLWA

e https://github.com/lwa-project/session_schedules

in LWA Swarm observations, preventing errors at a single LWA station from arresting interferometry runs. Observations are carried out independently at each LWA station, and then the data are automatically delivered back to the ELWA software correlator at the LWA UCF. After all data from an observation has been delivered, the correlator assembles a job queue from the available uncorrelated observations. Metadata files delivered with the data from each station are parsed to produce a correlator configuration file for each scan, containing information about the desired channel bandwidth, integration length, output polarization basis, and estimated clock offsets for each LWA station (and/or VLA antenna for ELWA runs).

Individual scans are then distributed to the three UCF computation nodes for correlation and are compiled into the generic FITS-IDI format. The correlated visibility data are then flagged for RFI using a basic SNR-based flagger and delivered to both the observer and LWA Data Archive. The correlator also produces quality assurance plots for observers to quickly inspect data quality, including plots of the fringe amplitude and phase as a function of time, and plots displaying a coarse window fit to delay and rate solutions. In this way, the LWA Swarm interferometry can be autonomously carried out, from observation to delivery of the final data product, simply using an IDF.

3. EXPECTED LWA SWARM SENSITIVITY

Although the LWA stations used for this survey do not have a uniform size, the expected sensitivity of the LWA Swarm can still be generalized using the standard radio telescope metrics of system temperature and aperture effective area. For an LWA station, the system temperature can be approximated using a power law relation that only depends on the observed wavelength in meters, λ , seen in Eq. 1 (S. W. Ellingson et al. 2009).

$$T_{sus}(\lambda) \approx 50\lambda^{2.56} \text{ K}$$
 (1)

The effective area of an LWA station, given in Eq. 2, depends on the number of antennas per array, N_{dip} , the impedance mismatch factor, ξ , the observed wavelength, λ , the beam center zenith angle, θ , and the antenna zenith gain, $G(\lambda)$ S. W. Ellingson et al. (2009).

$$A_{eff} = N_{dip} \times \xi G(\lambda) \frac{\lambda^2}{4\pi} \cos^{1.6}(\theta)$$
 (2)

If we assume that each LWA station has approximately the same system temperature according to Eq. 1, and compute the effective area of each station using Eq. 2. We may calculate the image plane sensitivity of the inhomogeneous LWA swarm using Eq. 3, from R. C. Walker (1989). Where k_b is the Boltzmann constant, $\Delta \nu$ is the observed bandwidth, Δt is the integration time, A_i represents the effective area of an individual array included in the calculation, and an extra factor of $1/\sqrt{2}$ is included to account for the dual polarization flux values reported in this study.

$$\Delta I = \frac{2k_b T_{sys}}{\sqrt{2\Delta\nu\Delta t}} \frac{1}{\sqrt{(\sum_i A_i)^2 - \sum_i A_i^2}}$$
(3)

In a dual-polarization 4-hour observing run, utilizing 32 MHz of effective bandwidth, and including one LWA Swarm station ($N_{dip} = 64$) plus two standard LWA stations ($N_{dip} = 256$), the idealized 74 MHz image plane sensitivity at zenith is expected to be ~ 5 mJy for high declination sources and ~ 20 mJy for our lowest declination sources. Given the lack of baselines for amplitude self-calibration, and

the prevalent impact of RFI and the ionosphere at these wavelengths, our objective here is to assess whether these theoretical limits are possible with the current and future LWA Swarm. For these reasons, we also excluded observing below 40 MHz in this survey, but fringes have been detected at sufficient signal-to-noise in the lower half of the LWA band with test observations (O. Wucknitz et al. 2024).

4. SURVEY SELECTION AND OBSERVATIONS

4.1. Calibrator Selection

In C. A. Taylor et al. (2025), test observations of radio galaxies commonly used as VLBI calibrators were conducted using the LWA Swarm to acquire timing solutions for the newly commissioned LWA-NA station. These pilot observations using the 3-element LWA Swarm in New Mexico (LWA1, LWA-SV, LWA-NA) showed fringe solutions of sufficiently bright radio sources were stable on minutes-long timescales. Since we were unable to resolve any background or field sources in these test observations, our preliminary estimates were that sources must have a **peak flux** at 74-MHz in the tens of Jansky range to use as a fringe fitting reference. Further, we identified that imaging compact radio sources required long observing tracks to improve (u, v) coverage.

Sources of interest for this survey were selected from the 74 MHz VLSSr catalog with **peak flux** > 40 Jy and Declination above 10°N (W. M. Lane et al. 2014). These constraints were imposed to maximize observing time above 30° elevation, allowing for approximately 8-hour observing tracks for this collection of targets (or \sim 6 hr in observations that include OVRO-LWA). Of the radio sources identified within these criteria, we eliminated the A-team sources (Cassiopeia A, Cygnus A, Taurus A, and Virgo A) from consideration due to their relative large angular size and extremely high flux density ($\theta_{Mj} > 50$ arcminutes and $S_{\nu} > 2$ kJy at 50 MHz; F. d. Gasperin et al. 2020). After removing the A-team sources, 36 targets fit these two conditions within the VLSSr. To these, we added 5 targets that are not included by the VLSSr selection criteria, but were previously detected during the commissioning observations of C. A. Taylor et al. (2025). These added targets were either below our declination cut-off (3C161, 3C298, 3C348) or the prescribed VLSSr **peak flux** threshold (3C41, 3C286).

4.2. Observations

Observations were conducted from Sept. 2024 - Mar. 2025 using the LWA Swarm interferometry mode, including the three LWA stations located in New Mexico: LWA1, LWA-SV, and LWA-NA. We select LWA tunings at center frequencies of 55 and 74 MHz, each with 19.6 MHz bandwidth, to provide slightly overlapped frequency coverage in the most sensitive LWA observing window. Each observing run consisted of 10-minute scans alternating between each target pointing in the nodding scheme typical of VLBI observations. As introduced in §4.1, our interferometry schedules were all approximately \sim 8 hr in total duration to achieve the longest continuous observing at sufficiently high elevation angle (\geq 30°). For this survey, baseband voltage data were correlated with a channel size of 19.14 kHz, at 0.5 s integration time, in the linear polarization basis.

All observations included one 'primary' calibrator plus 1-2 nearby 'target' calibrators from our sample. Primary calibrators were selected based on performance during the commissioning of LWA-NA and their reliability in providing high signal-to-noise fringe fitting solutions; they are 3C 48, 3C 147, 3C 196, 3C 254, 3C 295, 3C 380, and 3C 409.

On March 2, 2025, the digital processor at the LWA1 station failed following a power outage to the array. This unit was custom-designed by the Jet Propulsion Laboratory in 2012, but with digital and analog backend upgrades for LWA1 and LWA-SV planned to begin later in 2025, we halted observing for the LWA Swarm Survey campaign. As a result of this failure, only 30 of the intended 41 sources were observed in this survey, and they are listed in Table 1. The following sources were unable to be observed due to the LWA1 backend failure: 3C 27, 3C 033, 3C 47, 3C 69, 3C 84, 3C 348, 3C 410, 3C 430, 3CR 431, 3C 433, 3C 468.1.

Due to the high latency in data transfer when using the OVRO-LWA station, it was excluded from all survey observations. A series of test observations of reliable calibrator sources was conducted concurrently with the survey to establish limits in the use of OVRO-LWA in LWA Swarm observations. Our only successful joint interferometry run was conducted on October 3rd, 2024, observing 3C123 and 3C147, over 6 hours to keep targets above the same elevation threshold as the calibrator survey. This observation provided strong fringes on only 3C147, which allowed us to estimate a geometric delay and clock offset correction for OVRO-LWA in the LWA Swarm correlator for future observations.

5. DATA CALIBRATION AND IMAGING STRATEGY

Standard VLBI techniques at cm wavelengths typically include several calibrators for a single target field to improve global fringe fitting and calibration solutions (F. R. Schwab & W. D. Cotton 1983; J. Moldón et al. 2015). A primary calibrator, generally an unresolved and bright radio source, is selected within a few degrees of the target field to preserve the assumption that the direction-dependent solutions are transferable. Fringe fitting of this calibrator allows the bulk contributions of errors in the assumed array geometry of the correlator, instrumental effects, and the modulations caused by the dynamic atmospheric lens to be removed. A secondary in-beam calibrator is then used to derive further refinements to the delay and phase solutions. Baseline amplitudes can be calibrated with precise measurements of the system temperature and sensitivity of each antenna, or by referencing to a known flux calibrator.

The framework for global fringe fitting and amplitude calibration for LWA Swarm observations is based on this strategy for cm VLBI, with exceptions made to accommodate LWA observing capabilities. At meter wavelengths, the ionosphere will introduce stronger direction-dependent effects than the typical tropospheric models applied to GHz VLBI observing. Furthermore, it is also not recommended to attempt global delay and rate referencing for sources with an angular separation exceeding a few degrees. Unfortunately, the number density of bright, unresolved continuum sources within the preliminary sensitivity of the LWA Swarm makes solution referencing at long angular distances a requirement in most observations. The current LWA Swarm mode also does not support commensal system temperature and sensitivity measurements to robustly calibrate the baseline amplitude variations, so we can only employ rudimentary amplitude scaling. However, the purpose of this study was not to perfect the calibration and imaging of LWA Swarm radio sources, but rather to ascertain the constraints to do so with the next iteration of the LWA Swarm.

Our calibration begins with the standard two-step fringe fitting scheme using the FRING task in the Astronomy Image Processing System (AIPS; E. W. Greisen (2003)). The global fringe fitting is performed on a 2-minute solution interval from a scan near the peak elevation for our primary calibrator, solved over coarse delay (± 4000 ns) and rate (± 400 mHz) windows. This solution is applied to all sources for the entire observation to remove the bulk delay and phase rate terms on each

baseline that are unaccounted for in the LWA Swarm Correlator a priori. The ELWA correlator output reference level is arbitrarily low and necessitates significant amplification to reference amplitudes to physical units without access to amplitude self-calibration, so at this stage we also apply an arbitrary gain factor of 10 to improve visualization of diagnostic plots throughout the following calibration steps. A second stage of fringe fitting is performed to make fine corrections for delay drift and the ionospheric effects on each baseline. This is done independently for both primary and target calibrators over the entire observation using a refined delay and rate window. The fraction of valid timing solutions found in these steps is a low-level assessment of whether a given source can be used in the future as a Swarm calibrator. In the few cases where a target calibrator could not be fringe fit, we interpolate the second stage of delay and phase solutions from the primary calibrator.

We completed this delay and phase calibration process for all survey observations in the default linear polarization basis(XX, YY), before converting the visibilities to the circular polarization (RR, LL) basis to test for a difference in performance. Both bases were consistent with the pilot Swarm observations, showing stable delay and phase solutions over minutes-long timescales, with equivalent signal-to-noise. We report our results here using the circular polarization basis.

Delay-calibrated data are manually flagged for strong RFI using the tasks POSSM and UVFLG, then the task BPASS is used to create bandpass tables for our data. This was done iteratively, removing narrowband RFI spikes on each baseline until all bandpass fits converged to a smooth profile. Within the selected band, the combined RFI flagging of the ELWA correlator pipeline and manual flagging processes on average accounted for approximately 1-5% total data loss. Fig. 1 and 2 show the typical bandpass spectrum after delay calibration and flagging for LWA Swarm observations.

To set the amplitude scale for survey observations, we apply a fixed set of scaling coefficients for each antenna, derived from solving the system of equations to equalize the baseline amplitudes of the 3-element Swarm. This fixed scale is referenced to the **peak flux** of 3C295, as observed at the start of the survey. 3C295 is assumed to have a **peak flux** of 128.86 Jy at 74 MHz (W. M. Lane et al. 2014). Amplitude calibrated visibility data are then averaged in frequency from 2048 × 19 kHz channels, to 40×0.85 MHz channels. **Imaging of targets in the survey was done using the iterative cleaning and self-calibration techniques described in the Difmap Cookbook^f to measure the peak flux and image noise statistics of each target source (M. Shepherd 1997). In Difmap, we average visibility data in time from 0.5 s to 4 s to improve the computation time as time-average smearing is negligible on this interval for all sources. Image plane noise, \sigma_{rms}, was computed using a large map in Difmap to completely include the primary beam of the standard-sized (2.3°) and swarm-sized (3.2°) LWA stations at 74 MHz.**

The use of this amplitude reference framework imposes errors in the reported **flux** of observed radio sources, so we do not place significance on them until follow-up is possible. With only three LWA stations available at the time of the survey and the prevailing impact of the ionosphere in our frequency range, there are significant amplitude errors that remain after calibration. In this work, we aim to demonstrate that arcsecond resolution imaging with mJy level rms noise is reasonable

f ftp://ftp.astro.caltech.edu/pub/difmap/difmap.html

and accessible to the LWA Swarm interferometer. After the deployment of two more swarm stations during 2025–2026, this pipeline will introduce amplitude self-calibration to improve overall sensitivity and imaging capabilities.

6. RESULTS

Here, we present the results of the first survey of calibrator sources for the LWA Swarm interferometer. The measured peak flux, rms noise, and first contour levels for the 30 targets observed in this survey are reported in Table 1. Their distribution across the sky can be seen in Fig. 3, and the postage stamp contour maps of each source are provided in Fig. 4.

The purpose of this survey was to collect a catalog of strong delay and rate calibrators for use in future LWA Swarm interferometry, so we evaluated the quality of radio sources observed to first order by the success fraction in the second stage of global fringe fitting in AIPS. This **evaluation** was **done** after removing the stable residual delays between the three LWA stations, typically on the order of $10^2 - 10^3$ nanoseconds. We then classified the calibration targets in Table 1 using a quality label, ranking sources as either 'A'-tier calibrators for sources with < 2% failed solutions, 'B'-tier calibrators with < 5% failed solutions, or 'Not Recommended' (NR) for targets with > 25% failed solutions.

Five of the targets observed were unsuccessful in finding stable solutions during secondary fringe fitting and fell into the NR quality category. Rather than applying severely discontinuous solutions, these targets were instead referenced in delay and phase to the primary calibrator included in those observations. This technique is used for higher frequency VBLI observing to help resolve fainter sources in a field, but atmospheric effects at the observed wavelength will impose limits on the angular distance scale for which solutions of this kind will be valid. For two of the sources, 4C 58.02 and 3C 41, it was possible to transfer solutions from 3C 48 and produce reasonable images of the target source. This primary calibration transfer was difficult for the other three sources where fringe fitting failed, 3C 134, 3C 244.1, and 3C 338, in which we still were able to image some component of these sources, but at significantly lower flux than expected. Due to the angular separation and lack of rigorous amplitude calibration in this survey, we take these five sources' results as an indication that solution transfer could be possible with a more sensitive LWA Swarm, but we do not recommend these sources as primary calibrators.

The typical (u, v)-coverage of a 3-station LWA Swarm interferometry run is shown in Fig. 5 using the survey observation of 3C 147 imaged in Fig. 4. It is evident from the (u, v)-coverage map for the current iteration of the LWA Swarm that the lack of intermediate length baselines severely limits our sensitivity at the tens of arcsecond scale. Most targets from the survey are seen as unresolved point sources with evidence of apparent structure attributed to phase and amplitude errors (exceptions to this statement are described in more detail in § 6.1). Aside from the sources that required delay-rate referencing (NR), all other target fields produced acceptable images of the radio source located at the pointing phase center for calibration purposes. A comparison of the theoretical and observed noise of survey images is presented in Fig. 6, where the noise level accessible to this LWA Swarm implementation measures several factors larger than the idealized estimates, but the trend indicated that the survey was limited in dynamic range to a factor of \sim 10 for even the brightest radio sources.

Difmap is not optimized natively for wide field-of-view imaging because it does not make corrections for direction-dependent projection effects. We expect that the errors introduced by our calibration scheme are likely to have of greater impact on the results of this study than the unaccounted-for

projection effects ignored when imaging using Difmap. Though our observation of 3C 286 from September 3rd, 2024, provides evidence that this statement may not hold for an expanded LWA Swarm. Here we saw compact flux components of nearby radio sources in dirty and clean maps, which were separated from the image phase center by tens of arcminutes, and were cross-referenced with the corresponding VLSSR postage stamp. For this field, we imaged 3C 286 in Difmap to produce a clean model from its postage stamp image seen in Fig. 4, then used the Difmap clean model to calibrate the visibilities using the task CALIB in AIPS. Next, the field was imaged using the task IMAGR with the DO3DIMAG setting to help mitigate imaging errors from the large beam size.

In this separate imaging strategy for the 3C 286 field, seen in Fig. 7, we detect 4 additional field sources with peak flux between 1-2 Jy. The noise statistics of this field are comparable to images made only using Difmap, with the important distinction that we can resolve more than just the small region about the phase reference, however, the relative flux of the field sources we detect around 3C 286 is not consistent with VLSSr peak flux measurements. For nearby sources b, d, and e, we expect this to primarily be a result of amplitude artifacts around the phase reference, which can have noise fluctuations at three times the rms, with peaks greater than 50% of the expected source intensity. Bandwidth smearing and primary beam attenuation affects are negligible at separation angles < 10 arcminutes, but for the brightest and most distant source, 4C 31.42, this is not the case. At 38 arcminutes from the phase center, 4C 31.42 incurs significant bandwidth smearing effects at 0.85 MHz/channel (I/I_0 = 0.45), and the primary beam of both standard- and swarm-sized stations further reduces overall sensitivity by $\sim 20\%$. Decorrelation of solutions outside the phase center could be an important contributing factor given the ionospheric effects at low frequency. Even with these considerations, the comparison is further complicated by the resolution mismatch of the VLSSr (75") and the LWA Swarm (\sim 12.5") synthesized beams, so it is challenging to completely reconcile the difference in reported peak flux.

6.1. Extended Sources

Three targets from the survey showed evidence of extended emission post-calibration. These targets, Fanaroff-Riley II galaxies 3C 20, 3C 123, and 3C 330, are discussed below.

3C 20

3C 20 can be easily resolved using the VLA, which reveals extending kinked jets to the southwest and northeast of the core, with documented hotspots within each radio jet. Our image in Fig. 4 shows a point-like core at the phase center, but also diffuse emission oriented in the direction expected for the southwestern lobe of 3C 20. Though the assumed jet in our images seems to extend approximately 1 arcminute from the compact core and is relatively uniform in flux, VLA images at GHz frequencies usually detect bright knots in each jet at arcsecond-scale separations, which we cannot resolve with confidence. We also do not detect the northeastern radio jet in this observation.

 $3C\ 123$

3C 123 contains two asymmetric radio lobes, each with distinct contorted shapes indicative of interactions with the intergalactic medium. In two observations of 3C 123, after calibration and manual flagging in Difmap, it was evident that the source flux was extended over many arcminutes.

In hopes of improving our sensitivity and resolution, we concatenated the individually calibrated visibilities of the two runs using the AIPS task DBCON, then imaged the combined observations to produce the image of 3C 123 in Fig 4. Even so, we see that components of the emission are resolving out, and clear evidence of negatively trending amplitudes can be found on all baselines. Further, the total flux we measure of the source is between 5–70% below the literature values for this target at the same frequency. Visual comparison with higher frequency images taken by the VLA shows that we do not see the same twisted radio lobes, and notably, we have not detected a northern radio lobe (under the assumption that our image looks more like the southern lobe). Like our images of 3C 20, we are missing one of the two radio lobes and assume that we lack the required sensitivity on arcminute spatial scales to image the extended structure of these sources.

3C~330

3C 330 exhibits symmetric radio jets, unlike the other two FRII galaxies, and was recently studied in detail using the ILT and published VLA observations (A. Lafontaine 2023). This source is frequently used at many wavelengths as a delay calibrator, and the ILT study remarked that 3C 330 is well matched for low-frequency VLBI observing, due to the brightness in the band, one arcminute lobe separation, and hotspot structure. Unlike the other two targets with similar morphology, 3C 330 appears consistent with observations at higher radio frequency and most notably with recent observations using the ILT at 120-166 MHz. The clean map produced using LWA Swarm observations, seen in Fig. 4, places the peak emission from each radio jet in the same locations seen by the ILT, but we lack the resolution to distinguish structure in the lobes or the necessary calibration to make a robust measurement of the source flux.

7. DISCUSSION

Of the 30 radio sources for the future LWA Swarm interferometer, 25 were found to be adequate for use as long baseline calibrator sources. Repeated observations of primary calibrators did not show consistency in baseline amplitudes between epochs. For example, 3C 196 was included as a primary calibrator in six interferometry observations included in this survey and produced an average **peak** flux of 81.6 ± 11.5 Jy. In light of the static flux calibration framework, variable ionosphere, and absence of baselines for amplitude closure, a total flux error of approximately 14% is a satisfactory outcome for the survey. However, it serves as additional evidence that a more sophisticated calibration framework is required for the upcoming LWA Swarm.

To quantify ionospheric impacts and fringe solution consistency in time, Fig. 8 shows the delay difference between Right and Left circular polarizations for one full observing run on the primary calibrator 3C 196. Solutions tend to be smoothly varying within a single scan when the ionosphere is stable, primarily at night, and this is representative of the results of both A- and B-ranked calibrators. Approximately an hour before sunrise, ionospheric heating already begins to have an impact on the stability of solutions, increasing the delay difference between polarizations by tens of nanoseconds, especially on the longer baseline to LWA-SV. Daytime scans retain a relatively smooth profile but show noticeably more dynamic behavior and with slightly increased standard deviation. Additional evidence is found in the unique 3C 286 dataset, which contained the most consistent baseline amplitudes and noise throughout the observation on all included sources (3C 286, 3C 295, 3C 298), despite the observation occurring completely during

daytime. This behavior is consistent with what we see in Fig 8, and implies that while nighttime observing is preferable to daytime observing, the transition period during the few hours around sunrise, when the ionosphere has not reached its diurnal equilibrium, results in the most unstable fringe solutions for the mid-latitude LWA Swarm. Efforts were made to align some observations with the day-night cycle to minimize this ionospheric contamination, but the instrument health at the time of data collection necessitated observing when possible, so most of our observations include this day-night atmospheric transition period.

The survey detected identifiable nearby faint radio sources in the 3C 286 field and evidence of structure in three other radio galaxies, but the current limited number of baselines and primitive calibration make it challenging to reliably image targets with extended structure or radio sources many arcminutes from the phase center. Although in some cases we phase reference sources to their primary calibrators to attempt imaging, sometimes 10s of degrees away, the results are not indicative of this being a reliable strategy with the current calibration pipelines. Furthermore, utilizing the combination of AIPS and Difmap for widefield imaging of sources separated from the phase reference was only possible in a single field with exceptionally stable baseline amplitudes. To improve upon this, an expanded LWA Swarm will need to develop an imaging framework with the capability to account for direction-dependent effects to fully utilize the large LWA beam sizes.

Based on the results from this survey, it may be possible to calibrate Swarm observations using an unresolved point source with a peak \mathbf{flux} of ~ 10 Jy, with an angular extent smaller than 40 arcseconds. Although this is highly subject to the source declination for aperture synthesis and the time of day of the observation. In Appendix A, we provide a procedure that can be followed to set up an interferometry observation with the LWA Swarm using the strategies developed during this survey.

Instrumentation challenges impacted the success of the survey, including digitizer failures at LWA-SV that prevented standard calibration for a minimum of 48 antennas, a GPS failure delaying observing with LWA1 for several weeks, and the eventual failure of the digital backend at LWA1 prematurely ending the survey. As a result of the survey interruption, we were unable to complete follow-up observations on these few fields where fringe solutions were unsuccessful. These operational challenges highlight the timeliness of ongoing backend upgrades to the New Mexico LWA through 2025 and 2026, and the under-construction swarm stations, LWA-MC and LWA-CS. Even so, the image plane rms noise of survey observations was only a few factors larger than the estimated theoretical noise, which we consider an optimistic result for the rebuilt LWA Swarm.

8. CONCLUSIONS

The results of this survey, and the ongoing expansions of the LWA Swarm, emphasize the need to refine the existing correlation, calibration, and imaging pipelines. The additional baselines of a 6-station LWA Swarm will increase the existing correlator computation time of a typical 8-hour observation from 16 hours to 3.3 days, reducing the duty cycle to $\sim 10\%$. A proposed LWA Swarm Correlator would redesign the existing ELWA correlator to increase the available computation and

storage resources, while converting the majority of job multiprocessing to interface with GPUs using the Bifrost (M. D. Cranmer et al. 2017).

The calibration and imaging for this survey was done manually in AIPS and difmap, and is based on techniques that have been successful with previous ELWA observations. Advances in computing have enabled improved techniques in VLBI data analysis at MHz-frequencies, thanks to efforts by the LOFAR and MWA collaborations, to alleviate the impact of atmospheric propagation effects and large field-of-view observing (L. K. Morabito et al. 2025). Working to incorporate newer conditioning software to improve our calibration and imaging is the logical progression for LWA Swarm data reduction, with the added complexity and sensitivity of the future system. Upgrades could incorporate software packages such as AOFlagger, a sophisticated RFI excision program (A. R. Offringa 2010), an advanced imager that includes instrumental and direction-dependent corrections like WSClean(A. R. Offringa et al. 2014), and a custom library to precondition incoming interferometer data, similar to the LOFAR Initial Calibration pipeline (F. de Gasperin et al. 2019). Implementation of these will improve the data quality of the LWA Swarm, allowing for improved recommendations for scheduling and data processing of future open-skies LWA Swarm observations.

The ratio of calibrator to science field scan duration was 1:1. This was motivated by the precedent of successful test observations and evidence that the dynamic ionosphere could require significant monitoring of primary calibrators to permit delay and rate referencing to fainter sources. Utilizing the multiple steerable beams available to LWA stations is one way that we can improve LWA Swarm performance, increasing observing time on the target field while also incorporating a diverse set of calibrator scans. Ideally, keeping one beam continuously pointed at the science field, while a second independent beam is concurrently scheduled to move between a series of calibrators throughout an LWA Swarm run. Though this strategy effectively doubles the compute and storage requirements of each observation, and will be contingent on the resources available to the LWA Swarm after hardware upgrades are concluded.

Equipped with arcsecond resolution, millijansky imaging sensitivity, and independently steerable 2-degree beams at 80 MHz, the upgraded LWA Swarm telescope will observe parameter spaces inaccessible by this survey. Priority science goals of the future LWA Swarm are oriented towards low-frequency survey astronomy, detection of time-domain astrophysical processes, and follow-up of transient sources from other radio telescopes. We plan to perform a follow-up survey expanding this list of reference calibrators to provide better coverage across the sky for all LWA Swarm interferometry and establish new flux limits for calibration and imaging.

The flexibility afforded by multiple independent beams at each station allows for science observing to be commensal with the next LWA radio survey, using this preliminary catalog of calibrators as a foundation of reference pointings. High resolution imaging with the LWA Swarm will contribute to multi-wavelength studies of variability and dynamical processes in AGN (A. J. Tetarenko et al. 2019; K. Ross et al. 2021), studying pulsar scattering profiles and pulsar wind nebulae around young pulsars (K. Bansal et al. 2019; A. Lyne et al. 2022), and contribute to research on the emerging class of long-period radio transients discovered by the MWA GLEAM-X survey, exhibiting a steep radio spectrum and periodic emission on timescales up to minutes in pulse duration (N. Hurley-Walker et al. 2022, 2023). The 6-station LWA Swarm will have the angular resolution necessary to improve

localizations of low-frequency radio emitters such as these, and contribute to characterizing a variety of astrophysical sources throughout the first phase of observing.

ACKNOWLEDGEMENTS

Construction of the LWA has been supported by the Office of Naval Research under Contract N00014-07-C-0147. Support for operations and continuing development of the LWA is provided by the Air Force Research Laboratory and the National Science Foundation under grants AST-2107845 and AST-2103707. Renovations of the LWA1 and LWA-SV stations is supported by NASA grant 80NSSC23K0610. This research was sponsored in part by the Air Force Office of Scientific Research (AFOSR) Lab Task 23RVCOR002. Support for construction of the LWA-NA station was provided by the Air Force Office of Space Research Lab Task 23RVCOR002.

Table 1. LWA Swarm Calibrator Survey Sources

Source ID	Quality	RA (J2000)	DEC (J2000)	S (Jy/beam)	$\sigma_{rms} \; (\mathrm{mJy/beam})$	S_1 (Jy/beam)
$4C 58.02^{a}$	NR	00 36 08.02	+58 55 49.6	19	71	1.0
3C 20	В	$00\ 43\ 08.71$	$+52\ 03\ 29.1$	21	22	0.6
$3C \ 41^{a}$	NR	$01\ 26\ 44.4$	$+33\ 13\ 11$	19	125	1.0
3C48	A	$01\ 37\ 41.41$	$+33\ 09\ 38.2$	92	181	2.3
3C 123	A	$04\ 37\ 04.46$	$+29\ 40\ 15.3$	59	129	3.0
$3C \ 134^{a}$	NR	$05\ 04\ 43.17$	$+38\ 06\ 30.4$	9	20	0.4
3C 147	A	$05\ 42\ 36.04$	$+49\ 51\ 07.9$	51	76	1.5
$3C\ 154$	A	$06\ 13\ 49.81$	$+26\ 04\ 38.6$	17	70	0.9
3C 161	A	$06\ 27\ 10.1$	-05 53 06	61	102	3.5
3C 196	A	$08\ 13\ 36.22$	$+48\ 13\ 02.5$	89	109	2.2
$3C\ 208$	A	$08\ 53\ 08.57$	$+13\ 52\ 54.3$	20	33	1.2
3C 216	A	09 09 33.50	$+42\ 53\ 48.3$	47	86	2.4
3C 234	A	10 01 48.69	$+28\ 47\ 07.3$	20	60	1.1
$3C\ 244.1^a$	NR	$10\ 33\ 33.76$	$+58\ 14\ 33.6$	15	53	0.8
$3C\ 254$	A	$11\ 14\ 38.02$	$+40\ 37\ 17.6$	30	93	1.8
$3C\ 268.1$	A	$12\ 00\ 22.55$	$+73\ 00\ 48.6$	22	50	1.2
3C 280	A	$12\ 56\ 57.16$	$+47\ 20\ 21.7$	28	47	0.9
$3C\ 286$	A	$13\ 31\ 08.28$	$+30\ 30\ 32.96$	29	55	0.8
$3C\ 295$	A	$14\ 11\ 20.24$	$+52\ 12\ 06.6$	112	107	2.8
3C 298	A	$14\ 19\ 08.18$	$+06\ 28\ 34.80$	93	112	2.5
$3C\ 309.1$	A	$14\ 59\ 08.39$	$+71\ 40\ 20.6$	32	41	1.6
3C 330	A	$16\ 09\ 36.56$	$+65\ 56\ 43.3$	18	29	0.7
$3C \ 338^{a}$	NR	$16\ 28\ 38.11$	$+39\ 33\ 01.8$	20	71	1.0
$3C\ 368.0$	В	$18\ 05\ 06.60$	$+11\ 01\ 31.3$	28	90	1.4
$3C \ 380$	A	$18\ 29\ 31.78$	$+48\ 44\ 46.16$	80	124	2.5
3C 388	В	18 44 02.38	$+45\ 33\ 29.62$	15	69	0.9
$3C \ 394$	В	$18\ 59\ 23.64$	$+12\ 59\ 08.4$	20	39	1.0
$3C\ 409$	A	$20\ 14\ 27.62$	$+23\ 34\ 55.8$	85	117	2.2
$3C\ 427.1$	В	$21\ 04\ 07.89$	$+76\ 33\ 09.7$	34	81	1.8
3C 438	В	21 55 52.23	+38 00 27.9	42	101	2.2

 $[^]a$ Calibrators unable to be fringe fit independently and required delay and phase referencing from a primary calibrator source.

Table 2. Log of the Observations

	LWA Swarm Survey
Start Date	2024-09-03
End Date	2025-03-02
Total Beam Hours	158
Sources Scheduled	41
Sources Observed	30
Calibrators Identified	25

9. FIGURES

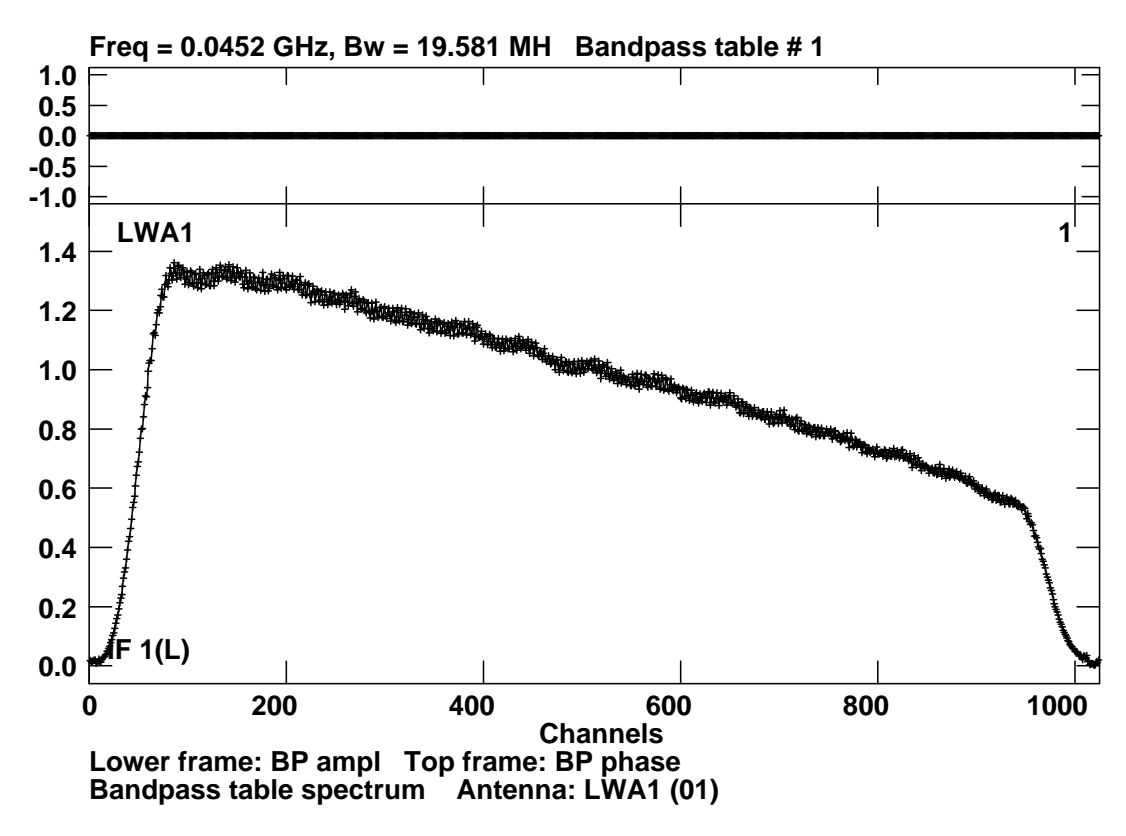


Figure 1. Standard bandpass profile for LWA Swarm interferometry observations. This figure shows the 55 MHz tuning at LWA1 for the left-hand circular polarized visibility data.

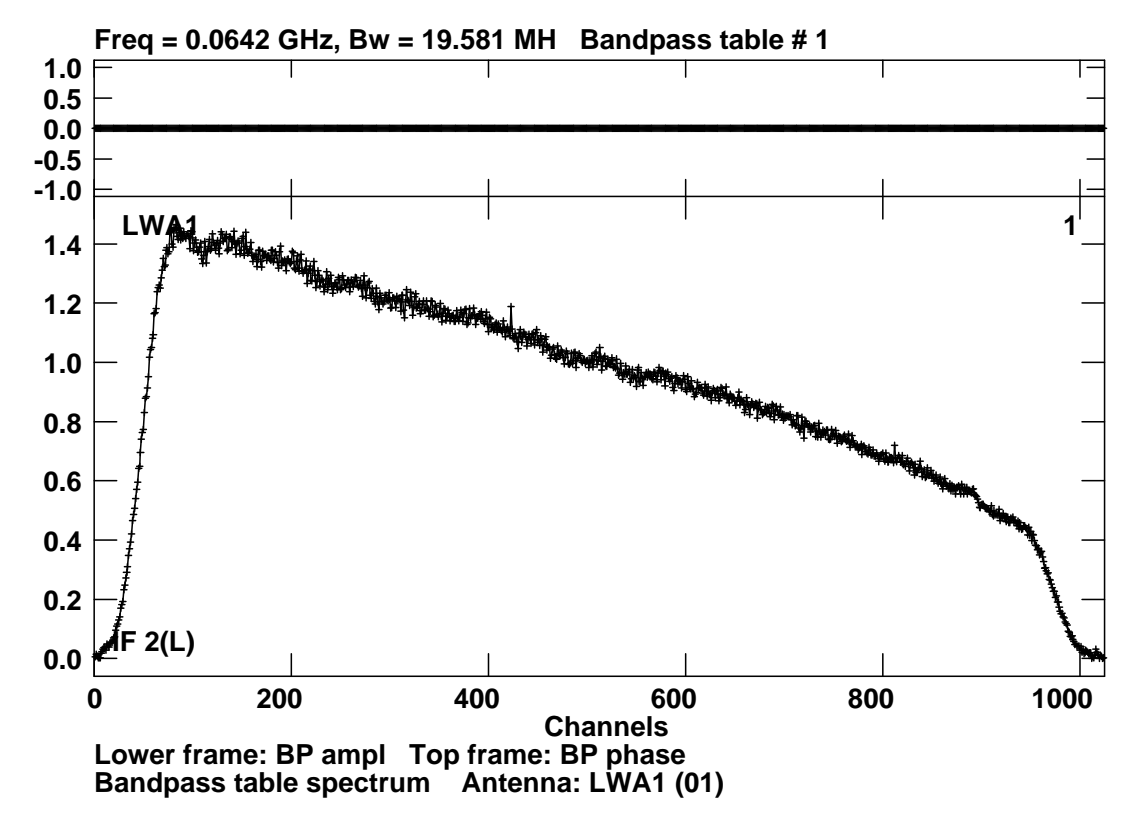


Figure 2. Same as Fig. 1, but plotting the bandpass for the 74 MHz tuning from LWA1.

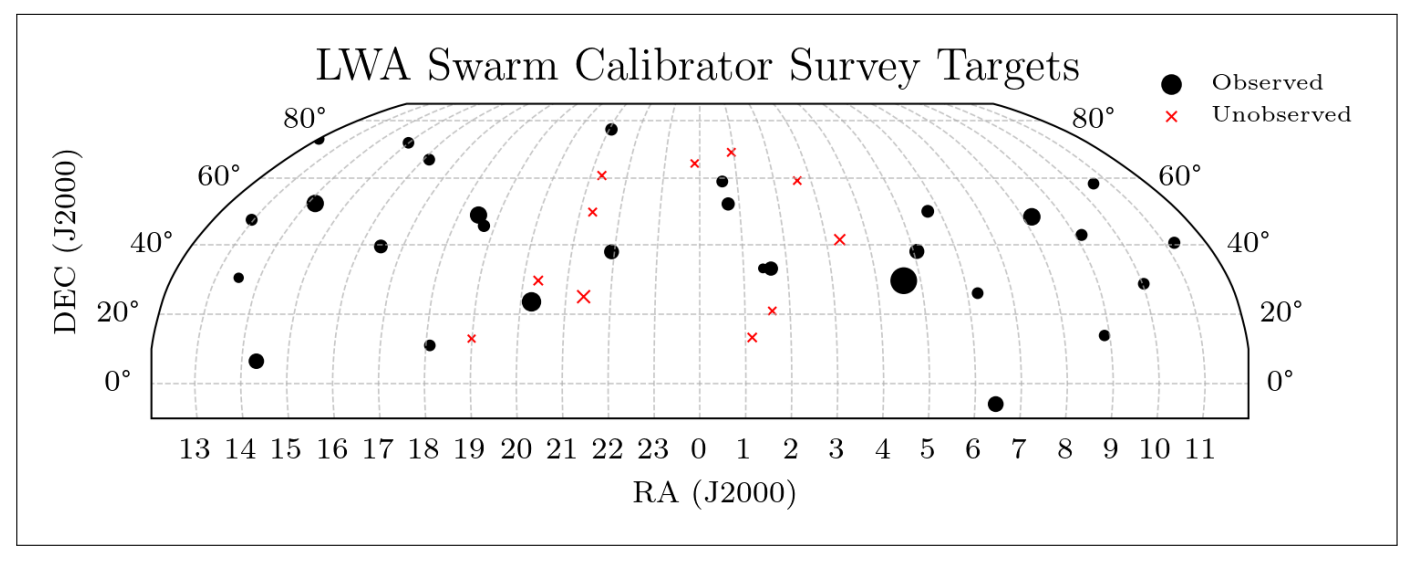


Figure 3. Map of calibrator sources observed in the LWA Swarm Calibrator Survey. Marker size is scaled by the **peak flux** observed by the LWA, and by the VLSSr **peak flux** at 74 MHz of each unobserved target(W. M. Lane et al. 2014).

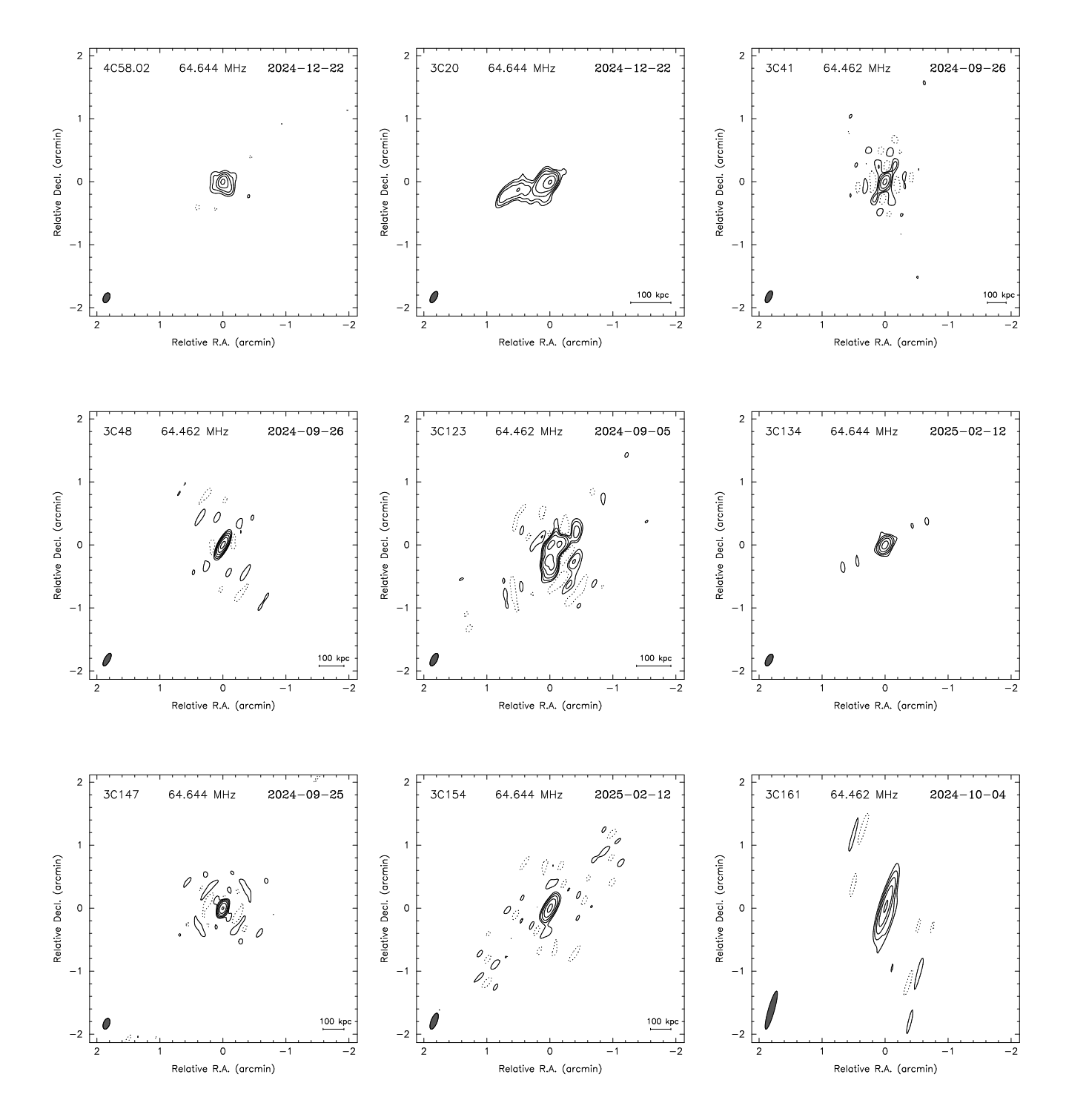


Figure 4. Postage stamp continuum images from the first LWA Swarm Calibrator Survey (45–84 MHz). Peak flux, rms noise, and first contour levels are listed in Table 1. Target sources' 3C identifier, post-calibration averaged center frequency, and observing epoch are listed at the top of each image. Beam size and size scale bars (if redshift is available) are shown in the bottom corners, assuming a Hubble constant of $H_0 \approx 73.04 \text{ km s}^{-1}\text{Mpc}^{-1}$ from the SH0ES collaboration(A. G. Riess et al. 2022).

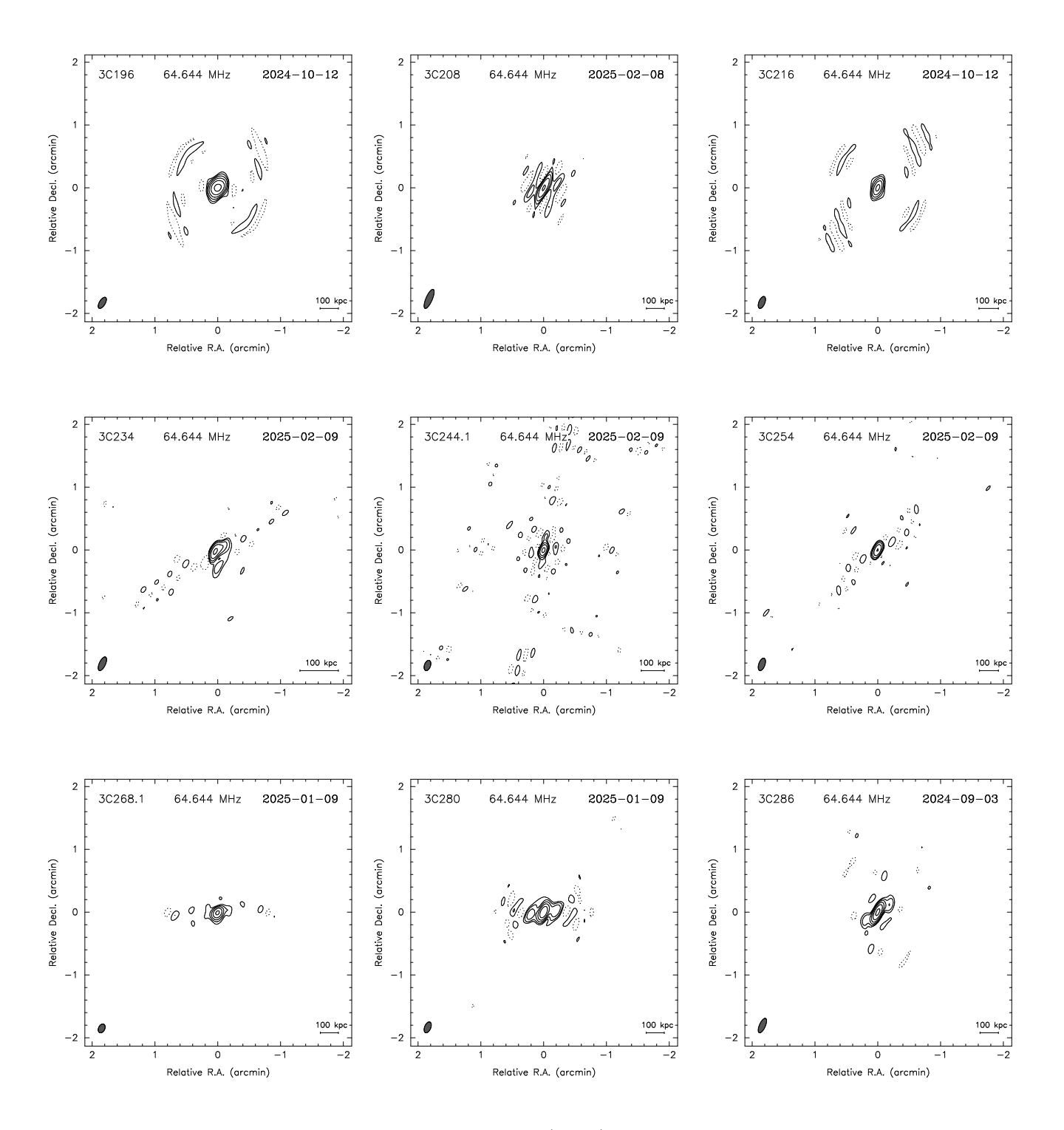


Figure 4. (cont.)

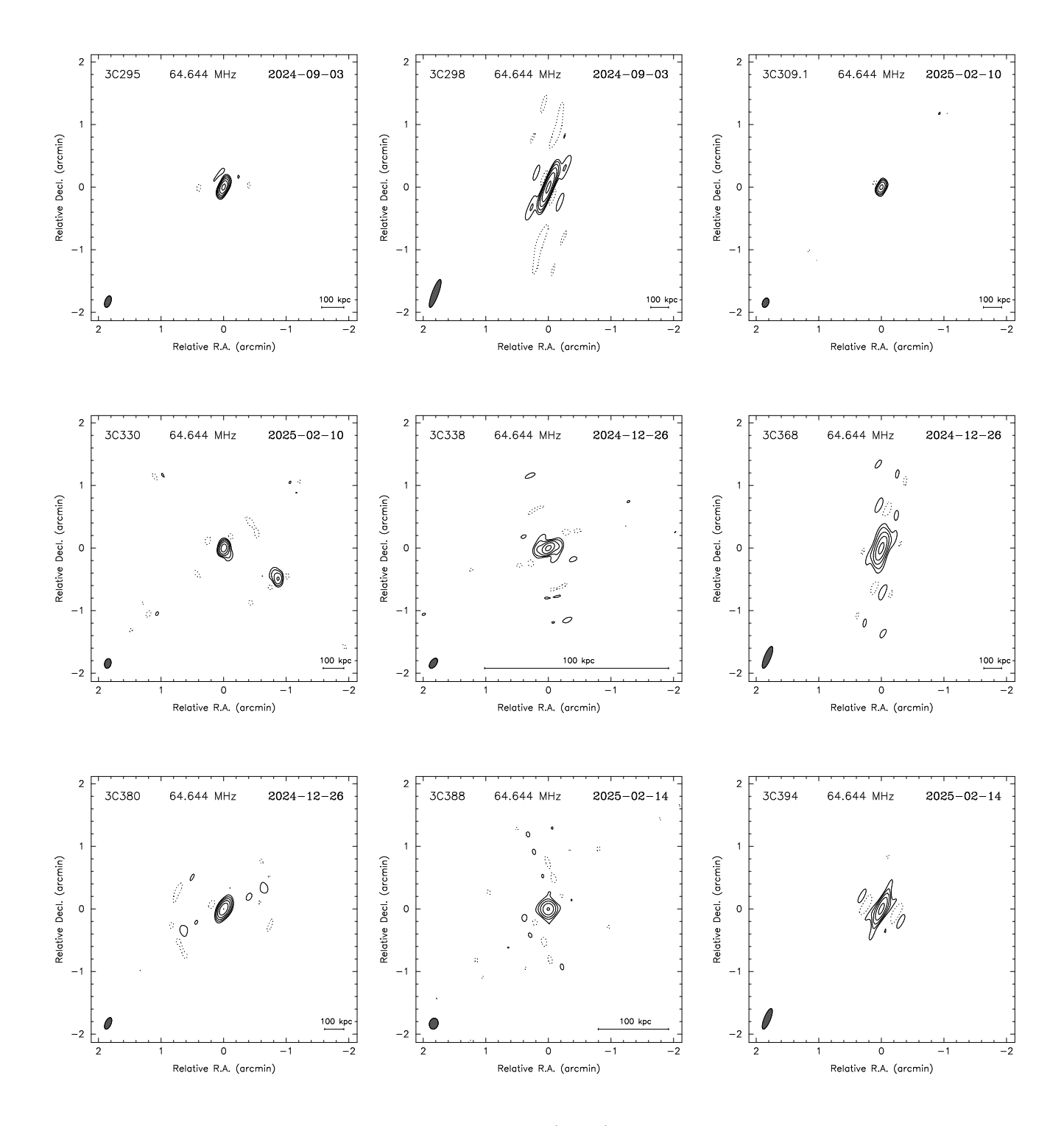


Figure 4. (cont.)

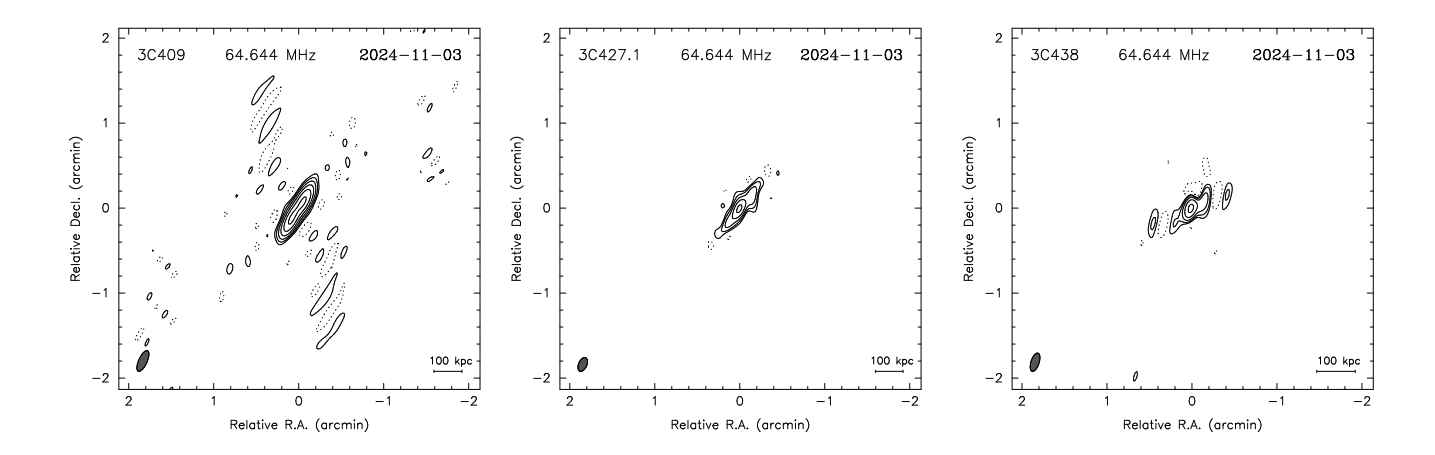


Figure 4. (cont.)

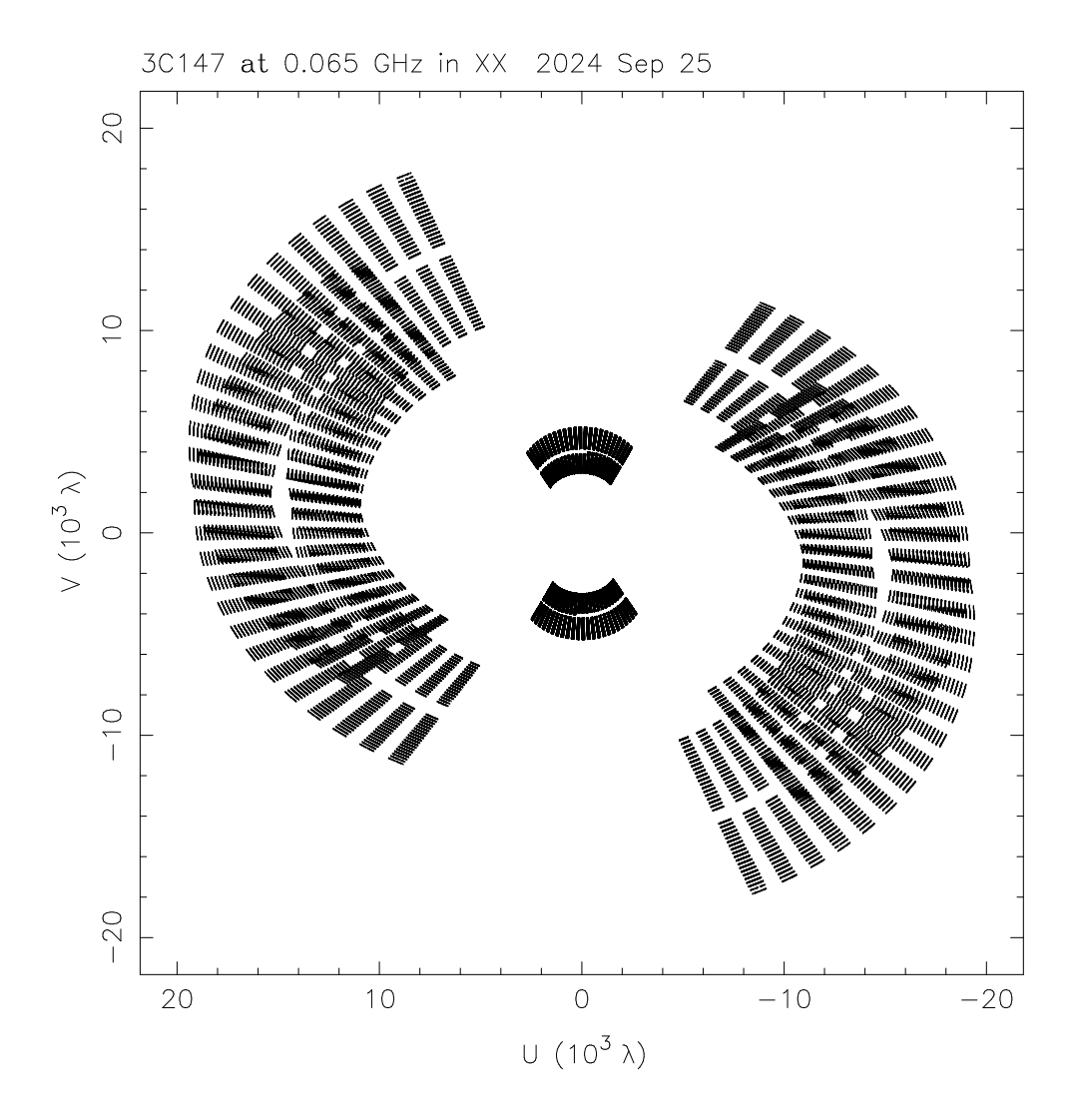


Figure 5. Example (u, v)-coverage for an 8-hour observing run of 3C147. Note that the final form of the data is split into 40 IFs to help with image synthesis, as seen in the coverage map. Image corresponding to this (u,v)-coverage map can be found in the Fig. 4 postage stamps.

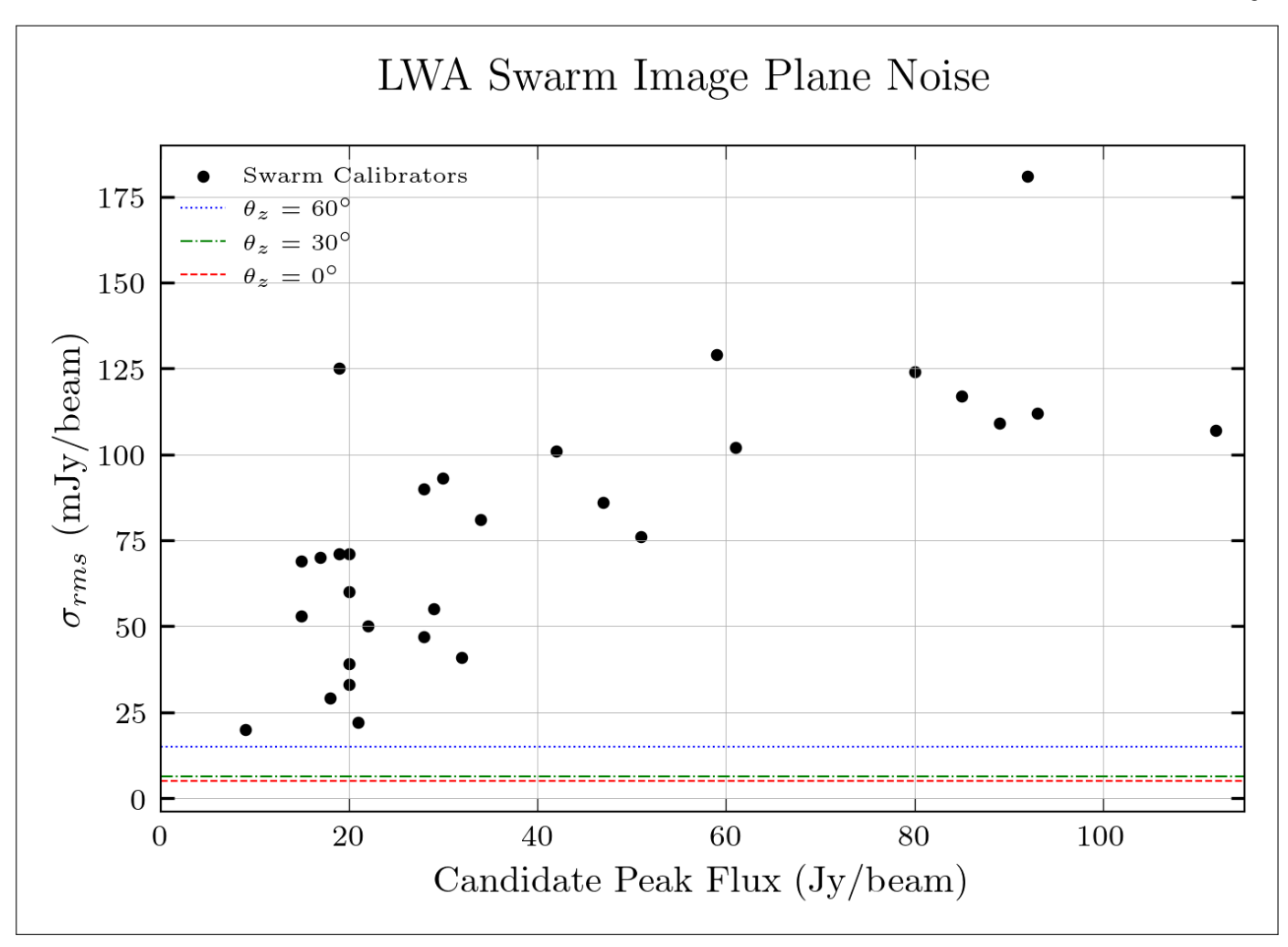


Figure 6. Image plane RMS noise is plotted against the **peak flux** for the radio sources observed in this survey from Table 1. Dashed horizontal lines correspond to the theoretical estimates for the 3-element LWA Swarm, including one Swarm station and two standard stations, using the equations in § 3 at practical zenith angles observed in the survey. Averaging across the survey observing band of 45–84 MHz, Eq. 3 estimates the noise to be approximately 7 mJy at $\theta_z = 0^{\circ}$, 9 mJy at $\theta_z = 30^{\circ}$, and 21 mJy at $\theta_z = 60^{\circ}$.

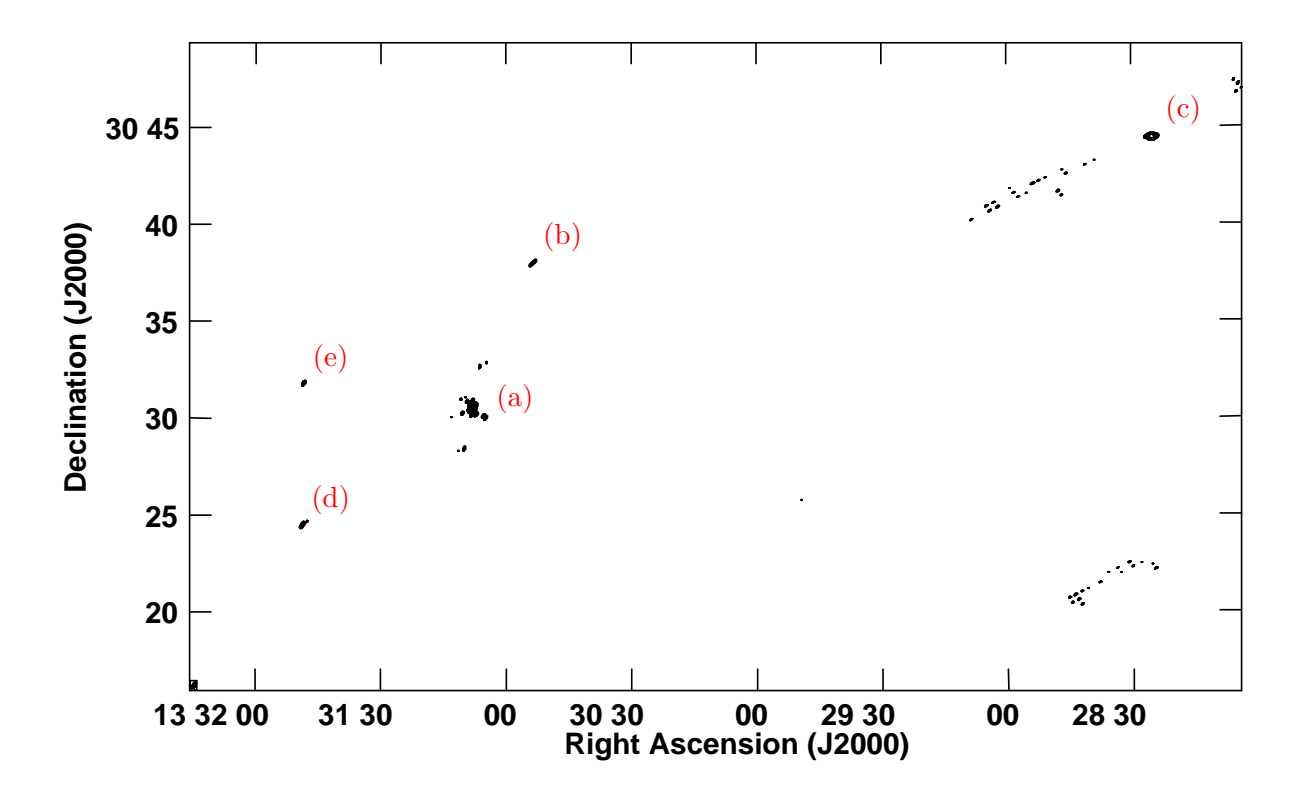


Figure 7. LWA Swarm 3C286 field observed on September 3, 2024. Radio source (a) 3C 286 is imaged with identified VLSSr field sources (b) NVSS J133053+303758, (c) 4C 31.42, (d) WISEA J133148.78+302928.9, and (e) WISEA J133148.48+303147.3.

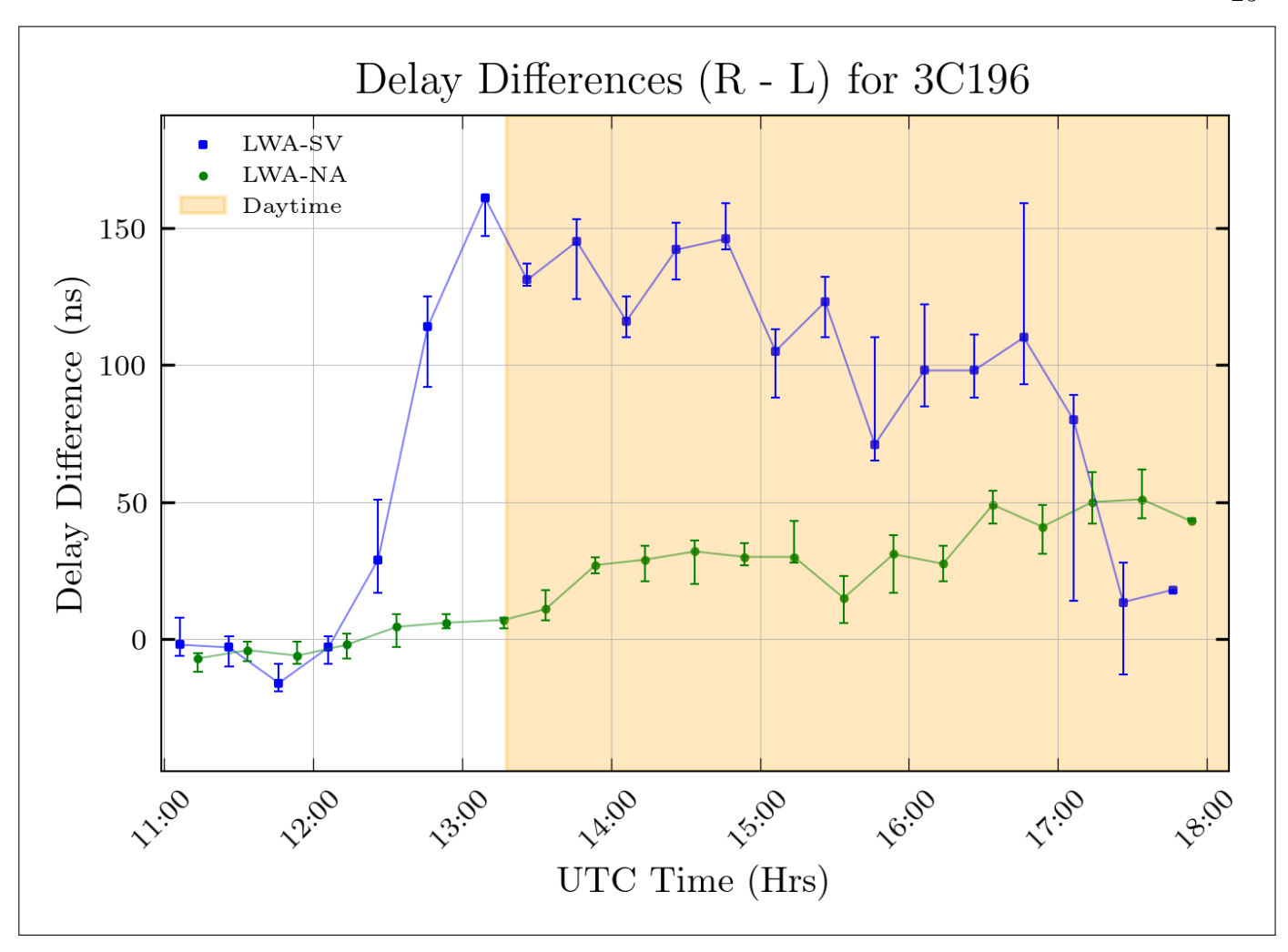


Figure 8. Delay drift comparison between the right and left circular polarization after global fringe fitting. Points represent the median value within the first and third quartiles, denoted by the range bars. Note that the comparative delay is stable until approximately 1 hour before sunrise, where the ionosphere begins to ionize and the delay solutions diverge due to differential Faraday effects.

498 APPENDIX

A. HOW TO PLAN AN LWA SWARM INTERFEROMETRY RUN

Given the current distribution of reliable LWA Swarm calibrators and our existing calibration pipeline, we make the following suggestions for planning an LWA Swarm observing run.

- 1. Identify a set of calibrators. The primary calibrator for bulk delay and rate referencing should be selected from the good sources in this survey. A secondary calibrator for delay and rate referencing should be located closer to the science field than the primary calibrator, but still have a peak flux of ~20 Jy at 74 MHz. Next, identify a third calibrator source < 3 degrees from the target for phase-only calibration. Ideally, an in-beam calibrator would be included among the selected calibrators.
- 2. Make test observations of calibrator sources, 10 minutes on each should be sufficient, to do a preliminary analysis of the selected calibrators for viability in fringe fitting.
- 3. Fringe fit this test observation using a variety of solution intervals to get an idea of how long your calibrator check scans need to be. A minimum of 2-4 minutes is recommended for primary calibrators, depending on the source declination.
- 4. Arrange the science observation to nod between the selected calibrators and the target field, using the solutions from the aforementioned test observation to motivate time allocation.
- 5. Include scans of the primary calibrator at a regular cadence, about every 1–2 hours, to provide delay and flux reference at various observing conditions.
- 6. Correlated products returned from the interferometry run will be available within a few days of the observation and can be further calibrated using the LWA Swarm Interferometry Guide (C. Taylor et al. 2025).

Availability permitting, two concurrent interferometry runs could be used to reduce the amount of interpolation required during calibration. In this strategy, one beam primarily follows the science field continuously, while the second beam performs all of the calibrator scans. With each beam periodically making check scans of the science field or primary reference calibrator for consistency. However, this strategy considerably increases the data reduction overhead and should be reserved for difficult-to-image fields.

REFERENCES

```
Morabito, L. K., Deller, A. T., Röttgering, H.,
    Bansal, K., Taylor, G. B., Stovall, K., & Dowell, J.
                                                         572
526
      2019, The Astrophysical Journal, 875, 146,
                                                          573
                                                                et al. 2016, Monthly Notices of the Royal
527
                                                                Astronomical Society, 461, 2676,
      doi: 10.3847/1538-4357/ab0d8f
                                                          574
528
                                                                doi: 10.1093/mnras/stw1501
    Cranmer, M. D., Barsdell, B. R., Price, D. C.,
                                                          575
529
                                                              Morabito, L. K., Jackson, N., de Jong, J., et al.
      et al. 2017, Bifrost: a Python/C++ Framework
                                                          576
530
                                                                2025, Astrophysics and Space Science, 370, 19.
                                                          577
      for High-Throughput Stream Processing in
531
                                                                doi: 10.1007/s10509-025-04406-x
                                                          578
      Astronomy, arXiv.
532
                                                              Offringa, A. R. 2010, Astrophysics Source Code
                                                          579
      http://arxiv.org/abs/1708.00720
533
                                                                Library, ascl:1010.017
                                                          580
    Davis, I., Taylor, G., & Dowell, J. 2020, Monthly
534
                                                          581
                                                              Offringa, A. R., McKinley, B., Hurley-Walker, N.,
      Notices of the Royal Astronomical Society, 494,
535
                                                                et al. 2014, Monthly Notices of the Royal
                                                          582
      4848, doi: 10.1093/mnras/staa988
536
                                                                Astronomical Society, 444, 606,
                                                          583
    de Gasperin, F., Dijkema, T. J., Drabent, A.,
537
                                                                doi: 10.1093/mnras/stu1368
      et al. 2019, Astronomy & Astrophysics, 622, A5,
538
                                                              Riess, A. G., Yuan, W., Macri, L. M., et al. 2022,
                                                          585
      doi: 10.1051/0004-6361/201833867
539
                                                                The Astrophysical Journal Letters, 934, L7,
                                                          586
    Dowell, J., & Taylor, G. B. 2018, Journal of
540
                                                                doi: 10.3847/2041-8213/ac5c5b
                                                          587
      Astronomical Instrumentation, 07, 1850006,
541
                                                              Ross, K., Callingham, J. R., Hurley-Walker, N.,
                                                          588
      doi: 10.1142/S225117171850006X
542
                                                                et al. 2021, Monthly Notices of the Royal
                                                          589
    Ellingson, S. W., Clarke, T. E., Cohen, A., et al.
543
                                                                Astronomical Society, 501, 6139,
                                                          590
      2009, Proceedings of the IEEE, 97, 1421,
544
                                                                doi: 10.1093/mnras/staa3795
                                                          591
      doi: 10.1109/JPROC.2009.2015683
545
                                                              Ruan, D., Taylor, G. B., Dowell, J., et al. 2020,
                                                          592
    Gasperin, F. d., Vink, J., McKean, J. P., et al.
                                                                Monthly Notices of the Royal Astronomical
546
                                                          593
      2020, Astronomy & Astrophysics, 635, A150,
                                                                Society, 495, 2125, doi: 10.1093/mnras/staa1305
547
                                                          594
      doi: 10.1051/0004-6361/201936844
                                                              Schwab, F. R., & Cotton, W. D. 1983,
548
                                                          595
    Greisen, E. W. 2003, in Information Handling in
                                                                Astronomical Journal (ISSN 0004-6256), vol. 88,
                                                          596
549
      Astronomy-Historical Vistas (Springer),
                                                                May 1983, p. 688-694., 88, 688
                                                          597
550
                                                              Shepherd, M. 1997, Astronomical Data Analysis
      109 - 125
                                                          598
551
                                                                Software and Systems VI, 125
                                                          599
    Groeneveld, C., Van Weeren, R. J., Miley, G. K.,
552
                                                              Taylor, C., Taylor, G., & Pezzaoili, S. 2025, Long
                                                          600
      et al. 2022, Astronomy & Astrophysics, 658, A9,
553
                                                                Wavelength Array Memo 228
                                                          601
      doi: 10.1051/0004-6361/202141352
554
                                                              Taylor, C. A., Dowell, J., Taylor, G. B., et al.
                                                          602
    Hurley-Walker, N., Zhang, X., Bahramian, A.,
555
                                                                2025, Journal of Astronomical Instrumentation,
                                                          603
      et al. 2022, Nature, 601, 526,
556
                                                                14, 2550003, doi: 10.1142/S2251171725500035
                                                          604
      doi: 10.1038/s41586-021-04272-x
557
                                                              Taylor, G. B., Ellingson, S. W., Kassim, N. E.,
                                                          605
    Hurley-Walker, N., Rea, N., McSweeney, S. J.,
558
                                                                et al. 2012, Journal of Astronomical
                                                          606
      et al. 2023, Nature, 619, 487,
559
                                                                Instrumentation, 1, 1250004,
                                                          607
      doi: 10.1038/s41586-023-06202-5
560
                                                                doi: 10.1142/S2251171712500043
                                                          608
    Lafontaine, A. 2023, PhD Thesis, University of
561
                                                              Tetarenko, A. J., Casella, P., Miller-Jones, J.
                                                          609
      Groningen
562
                                                                C. A., et al. 2019, Monthly Notices of the Royal
                                                          610
    Lane, W. M., Cotton, W. D., van Velzen, S., et al.
563
                                                                Astronomical Society, 484, 2987,
                                                          611
      2014, Monthly Notices of the Royal
564
                                                                doi: 10.1093/mnras/stz165
                                                          612
      Astronomical Society, 440, 327,
565
                                                              Tremou, L., Schinzel, F., Long, R., Ramzel, J., &
                                                          613
      doi: 10.1093/mnras/stu256
566
                                                                Werts, D. 2024, EVLA Memo #233
                                                          614
    Lyne, A., Graham-Smith, F., & Stappers, B. 2022,
567
                                                              Walker, R. C. 1989, in Very Long Baseline
                                                          615
      Pulsar Astronomy, 5th edn., Cambridge
                                                                Interferometry: Techniques and Applications,
568
                                                          616
      Astrophysics (Cambridge University Press)
                                                                ed. M. Felli & R. E. Spencer (Dordrecht:
569
                                                          617
    Moldón, J., Deller, A., Wucknitz, O., et al. 2015,
                                                                Springer Netherlands), 163–182,
570
                                                          618
                                                                doi: 10.1007/978-94-009-2428-4_9
      Astronomy & Astrophysics, 574, A73
                                                          619
571
```

Wayth, R. B., Tingay, S. J., Trott, C. M., et al.
2018, Publications of the Astronomical Society
of Australia, 35, e033, doi: 10.1017/pasa.2018.37
Wucknitz, O. 2010,

Wucknitz, O., Bassa, C. G., Bondonneau, L., et al. 2024, in Proceedings of the 16th EVN Symposium, ed. E. Ros, P. Benke, S. A. Dzib, I. Rottmann, & J. A. Zensus, 199–202